

Tuning the Adsorption Properties of Metal-Organic Frameworks through Co-adsorbed Ammonia

Eric Chapman,^{1†} Saif Ullah,^{1†} Hao Wang,² Liang Feng,⁴ Kunyu Wang,⁴ Hong-Cai Zhou,⁴ Jing Li,² Timo Thonhauser,^{1*} and Kui Tan^{3*}

¹Department of Physics and Center for Functional Materials, Wake Forest University, Winston-Salem, NC 27109

²Department of Chemistry and Chemical Biology, Rutgers University, Piscataway, NJ 08854

³Department of Materials Science & Engineering, University of Texas at Dallas, Richardson, TX 75080

⁴Department of Chemistry, Texas A&M University, College Station, TX 77843

ABSTRACT: In this work, we report a novel strategy to increase gas adsorption selectivity of metal organic framework materials by co-adsorbing another molecular species. Specifically, we find that addition of tightly bound NH_3 molecules in the well-known metal-organic framework MOF-74 dramatically alters its adsorption behavior of C_2H_2 and C_2H_4 . Combining *in situ* infrared spectroscopy and *ab initio* calculations, we find that—as a result of co-adsorbed NH_3 molecules attaching to the open metal sites— C_2H_2 binds more strongly and diffuses much faster than C_2H_4 , occupying the available space adjacent to metal-bound NH_3 molecules. Most remarkably, C_2H_4 is now almost completely excluded from entering the MOF once C_2H_2 has been loaded. This finding dispels the widespread belief that strongly co-adsorbed species in nano-porous materials always undermine their performance in adsorbing or separating weakly bound target molecules. Furthermore, it suggests a new route to tune the adsorption behavior of MOF materials through harnessing the interactions among co-adsorbed guests.

KEYWORDS: MOFs, co-adsorption, selectivity, infrared spectroscopy, and *ab initio* calculation

Introduction

Understanding fundamental mechanisms of molecular co-adsorption in nano-porous materials such as metal-organic frameworks (MOFs) is of key importance for realizing their potential in sorption-based storage and separation applications—yet, remarkably little is known about them due to the limitations of *in situ* characterization.¹⁻⁷ Co-adsorbed impurities are usually regarded as detrimental in adsorption processes because they occupy or co-adsorb at the available adsorption sites and thus deteriorate the materials' sorption performance for the target molecules.^{3, 6, 8-14} In our previous work,¹⁵ we found that—contrary to the prevailing assumption that competing adsorbates such as H_2O or NH_3 are undesirable in the context of adsorption applications—they can also play an important role in stabilizing co-adsorbed molecules such as CO , CO_2 , and SO_2 by creating additional diffusion barriers via H-bonding interactions through the MOF channel.¹⁵ This synergistic effect is particularly emphasized in the prototypical material MOF-74 [$\text{M}_2(\text{dobdc})$, $\text{M}=\text{Co}^{2+}$, Ni^{2+} , Mg^{2+} , etc and

$\text{dobdc}=2,5\text{-dihydroxybenzenedicarboxylic acid}$], which contains a high density of coordinatively unsaturated metal centers (also called open metal sites) along its hexagonal channels, which can adsorb weakly bound molecules (see Fig. 1).^{10, 16-21} In MOF-74, post-loaded NH_3 successfully traps other preloaded oxygen-containing molecules inside the MOF.¹⁵ On the other hand, the diffusion of hydrocarbons such as C_2H_4 and C_3H_6 is not strongly impeded due to their lack of oxygen to form hydrogen-bonding interactions.

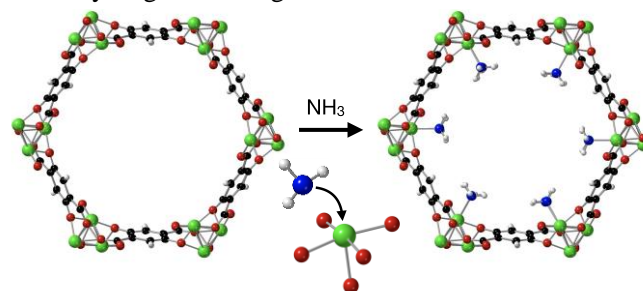


Figure 1. MOF-74 structure with open metal sites on pyramid oxide clusters terminated by NH_3 . Green = Co, red = O, black = C, blue = N, white = H.

In this work, we report another surprising finding that co-adsorbed NH_3 alters the binding energy and diffusion barrier of C_2H_2 and C_2H_4 to a different degree within the MOF channels, leading to a notable preferential adsorption of C_2H_2 over C_2H_4 . This finding is entirely unexpected as their binding energies in pristine MOF-74 is very similar, resulting in very low selectivity of C_2H_2 over C_2H_4 .^{17-18, 22} *In situ* infrared spectroscopy is employed since it allows us to directly monitor the kinetics of multi-components co-adsorption based on their unique fingerprint bands and further probe molecular adsorption geometries and guest-guest interactions,²³ which are inaccessible through other methods such as adsorption isotherm or breakthrough measurement. Our experimental results are coupled with *ab initio* calculations to unveil the dynamic adsorption behavior of mixed gases. We select Co-MOF-74 analogues to study the co-adsorption of $\text{C}_2\text{H}_2/\text{C}_2\text{H}_4$ gas mixtures in both pristine and NH_3 -loaded samples because they were previously found to have the strongest interaction with both acetylene and ethylene owing to the high polarizability of the open Co^{2+} ions.¹⁷⁻¹⁸ The similarity of their

binding energy (~ 50.1 for C_2H_2 and ~ 47 kJ/mol for C_2H_4 ¹⁷⁻¹⁸) in the pristine MOF-74 structure makes their separation a difficult task.²² In an effort to alter the binding landscape, we have chosen to terminate the open metal sites with NH_3 , which binds strongly through the donation of its lone pair to form a coordinative bond.⁹ Note that the volatile NH_3 is preferable over H_2O in our present study since the former binds more strongly within MOF-74 (see Fig. S3). Moreover, H_2O easily forms hydrogen-bonded clusters that occupy the entire channel and block other molecules from entering inside.²⁴

Experimental section

Sample preparation

Co-MOF-74: Co-MOF-74 was synthesized on the basis of a previous report.²⁵ $Co(NO_3)_2 \cdot 6H_2O$ (75 mg), Linker DOBDC (15 mg), EtOH (0.5 mL), H_2O (0.5 mL), and DMF (6 mL) were charged into a 20 mL Pyrex vial. The mixture was heated in 120 °C oven for 24 h. After cooling down to room temperature, the red–orange Co-MOF-74 were harvested. The MOF materials were further washed thoroughly with DMF and then exchanged by EtOH for 3 days, during which the solvent was decanted and freshly replenished three times every day. Then the MOF sample was stored in a N_2 glove box.

Mg-MOF-74: Mg-MOF-74 was synthesized on the basis of a previous report.²⁶ $Mg(NO_3)_2 \cdot 6H_2O$ (80 mg), Linker DOBDC (18 mg), EtOH (0.5 mL), H_2O (0.5 mL), and DMF (7.5 mL) were charged into a 20 mL Pyrex vial. The mixture was heated in 120 °C oven for 24 h. After cooling down to room temperature, the yellow Mg-MOF-74 were harvested. The MOF materials were further washed thoroughly with DMF and then exchanged by EtOH for 7 days, during which the solvent was decanted and freshly replenished three times every day. Then the MOF sample was stored in a N_2 glove box.

The crystal structure of Co, and Mg-MOF-74 was measured by PXRD as shown in Fig. S1. The XRD diffraction pattern of the samples we studied is in agreement with literature report.²⁷ Thorough solvent exchange, the BET surface area, derived from N_2 adsorption isotherm reaches 1200 and 1430 m^2/g for Co, and Mg-MOF-74 (see Fig. S2), respectively, consistent with the values (835-1292 m^2/g of Co-MOF-74,^{16, 28-30} and 1174-1542 m^2/g of Mg-MOF-74^{16, 28-29, 31}) reported in previous studies.

In situ Infrared Spectroscopy: *in situ* IR measurements were performed on a Nicolet 6700 FTIR spectrometer equipped with a liquid N_2 -cooled mercury cadmium telluride MCT-A detector. The sample of MOF compound (~ 5 mg) was pressed onto a KBr pellet and placed into a vacuum cell placed at the focal point of the sample compartment of the infrared spectrometer. The cell is connected to different gas lines including C_2H_2 , C_2H_4 , NH_3 , and C_2H_2/C_2H_4 mixed gases (50%/50%) purchased from Matheson. The samples were activated by evacuation (base pressure < 20 mTorr) at 180 °C for at least 3 h to remove adsorbed solvents or H_2O (monitored by taking in-situ IR spectra) and then cooled back to room temperature for recording the reference spectrum and subsequent hydrocarbon adsorption measurement. To obtain a sample with the

metal sites fully passivated by NH_3 , namely $NH_3@MOF-74$, the activated sample was exposed to ~ 50 Torr NH_3 for ~ 5 min and subsequently evacuated for ~ 15 h to remove weakly bound NH_3 at the secondary sites. Hydrocarbon adsorption measurement was further conducted on the $NH_3@MOF-74$ samples.

Ab initio calculations: Our *ab initio* calculations were performed at the density functional theory level, using the plane-wave code VASP³²⁻³³ and PAW pseudopotentials. To capture important non-covalent interactions, we made use of the vdW-DF1 method.³⁴⁻³⁷ The kinetic energy cutoff was set to 600 eV; forces were converged to within 1 meV/atom with a SCF criterion of 10^{-6} eV. Spin polarized calculations were performed with the antiferromagnetic (AFM) ordering for Co.³⁸ Gamma-point sampling is found to be sufficient due to the large unit cell size (108 atoms for the pristine empty MOF). Binding energies are calculated as suitable differences of energies between the loaded MOF and empty MOF and guest molecule(s). Diffusion barriers were calculated with the help of transition-state search algorithms. The barrier is then calculated by simulating the diffusion of the molecules along the channel axis. We used the climbing image nudged elastic band (cNEB) method for this purpose.³⁹⁻⁴⁰

Results and discussion

We start with spectroscopic measurements of the single-phase C_2H_2 and C_2H_4 adsorption in pristine Co-MOF-74 as a reference. After loading C_2H_2 at 200 Torr at 25 °C, the characteristic bands $\nu(C_2H_2)$ and $\delta(C_2H_2)$ were detected at 3240 and 760-736 cm^{-1} ,⁴¹ respectively (see Fig. 2a and Fig. S4). The deformation band $\delta(C_2H_2)$ was split into two components at 760 and 736 cm^{-1} , which suggests that acetylene molecules are adsorbed parallel to the plane of the cobalt oxide pyramid clusters,¹⁸ forming π -complexes with Co^{2+} and leading to the degeneracy lifting of the in-plane and out-of-plane mode, which is confirmed by our *ab initio* calculations. The relative intensity of in-plane mode at 760 cm^{-1} gradually diminishes as the loading increases, which could result from the lateral interaction among guest C_2H_2 .⁴²⁻⁴³ After fully evacuating C_2H_2 under vacuum, the sample was further exposed to 200 Torr C_2H_4 , resulting in an intense peak at 973 cm^{-1} that corresponds to the deformation band δ of π -bonded C_2H_4 on the Co^{2+} centers (see Fig. 2a).⁴⁴ The stretching band of adsorbed C_2H_4 appears at 2937 cm^{-1} with much weaker intensity (see Fig. S4b). Note that the spectra of both ethylene and acetylene are dominated by the C–H deformation bands⁴⁵, and our analysis here will focus on these modes. At a pressure of 200 Torr and temperature of 25 °C, the occupancy of C_2H_2 and C_2H_4 reaches ~ 1 and 0.8 molecules, respectively, per Co^{2+} site, based on previous sorption measurements.¹⁷⁻¹⁸ After evacuating the adsorbed C_2H_4 molecules at 25 °C (see Fig. S5b), further adsorption measurements of a C_2H_2/C_2H_4 mixture (~ 200 Torr/ ~ 200 Torr) were performed on the same sample. Figure 2a shows that C_2H_2 and C_2H_4 are co-adsorbed

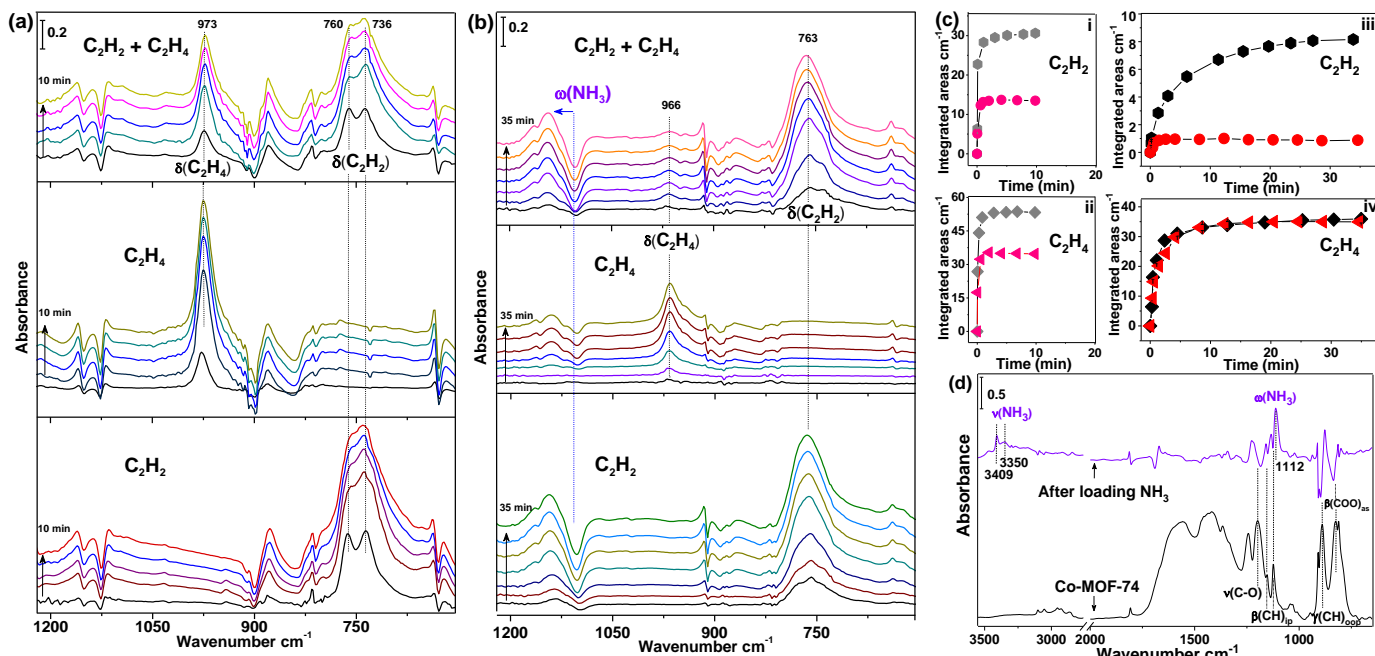


Figure 2. (a) and (b) Spectral evolution of the deformation band δ of adsorbed C_2H_2 and C_2H_4 in pristine (a) and NH_3 -loaded Co-MOF-74 (b) upon exposure to single C_2H_2 (bottom), C_2H_4 (middle) and mixed C_2H_2/C_2H_4 (top) at 200 Torr/200 Torr. The spectra are referenced to the pristine and NH_3 -loaded Co-MOF-74 in vacuum. (c) Evolution of integrated areas of $\delta(C_2H_2)$ and $\delta(C_2H_4)$ bands in single and mixed components adsorption in pristine Co-MOF-74 (i, ii; gray hexagon and diamond for C_2H_2 and C_2H_4 in their single phase, pink circle and triangle for C_2H_2 and C_2H_4 in their mixed phases) and $NH_3@Co-MOF-74$ (iii, iv; black hexagon and diamond for C_2H_2 and C_2H_4 in their single phase, red circle and triangle for C_2H_2 and C_2H_4 in their mixed phases). (d) Difference spectrum of NH_3 -exposed Co-MOF-74 upon gas loading at 50 Torr for ~ 5 min and subsequently evacuating gas phase for ~ 15 h (top), compared with the spectrum of activated Co-MOF-74 (bottom), referenced to the blank KBr pellet in vacuum.

inside Co-MOF-74, typified by in-situ growth of their characteristic bands δ at 973, 760 and 736 cm^{-1} . The intensities of the $\delta(C_2H_4)$ and $\delta(C_2H_2)$ bands in the gas mixture decrease by $\sim 60\%$ and $\sim 30\%$, respectively, compared with their values in the single-component adsorption (see Fig. 2a and 2c).

After fully desorbing C_2H_2 and C_2H_4 from pristine Co-MOF-74, ~ 50 Torr NH_3 gas was introduced to passivate the active metal sites. The characteristic band of adsorbed NH_3 was detected near 3409 and 1112 cm^{-1} , which correspond to the N–H stretching (ν) and wagging (ω) mode (see Fig. 2d).⁴⁶ The adsorbed NH_3 is strongly bound inside the MOF due to the formation of a coordinative M–N bond, as indicated by the large blue shift of the $\omega(NH_3)$ band with respect to the gas-phase value at 950 cm^{-1} .⁴⁶ The region from 1600 to 800 cm^{-1} in the difference spectrum of Figure 2d is also characterized by strong perturbations of the MOF's phonon modes due to NH_3 adsorption (see Table S1). Upon evacuation overnight at room temperature, both $\nu(NH_3)$ band at 3409 cm^{-1} and $\omega(NH_3)$ at 1112 cm^{-1} remain almost unchanged (see Fig. S6). C_2H_2 at 200 Torr was loaded again into the sample with co-adsorbed NH_3 , referred to here as $NH_3@Co-MOF-74$. The spectra were recorded as a function of time to monitor the kinetics of the adsorption. Considerable $\nu(C_2H_2)$ and $\delta(C_2H_2)$ bands of ad-

sorbed C_2H_2 were observed at 3190 and 763 cm^{-1} (see Fig. 2c and S7a). Figure 2c shows that C_2H_2 adsorbs slower in $NH_3@Co-MOF-74$ compared to the pristine sample. The $\delta(C_2H_2)$ band in $NH_3@Co-MOF-74$ displays only one component at higher loading, indicating a modification of the binding configuration due to the presence of NH_3 ; its total intensity decreases by $\sim 35\%$ compared with that in pristine sample (see Fig. 2c). The $\omega(NH_3)$ band is also perturbed upon loading C_2H_2 rather than decreased in intensity (see Fig. 2b and discussed further below), indicating that C_2H_2 interacts with (but does not displace) co-adsorbed NH_3 . Note that complete C_2H_2 desorption is still possible under vacuum (see Fig. S8a). Loading C_2H_4 into $NH_3@Co-MOF-74$ was performed in the same manner and monitored by tracking the $\delta(C_2H_4)$ band that appears at 967 cm^{-1} and exhibits a red shift of 7 cm^{-1} with respect to the value in pristine MOF-74. C_2H_4 adsorption is obviously decreased and slowed down in $NH_3@Co-MOF-74$ compared with pristine Co-MOF-74, that is, within ~ 30 min it only reaches $\sim 25\%$ of the initial loading observed in pristine Co-MOF-74. After evacuating the sample again of adsorbed C_2H_4 by pumping under vacuum (see Fig. S8b), a C_2H_2/C_2H_4 mixture (~ 200 Torr/ ~ 200 Torr) was introduced to study the co-adsorption in $NH_3@Co-MOF-74$. To our surprise, C_2H_4 adsorption is strongly suppressed in the gas-

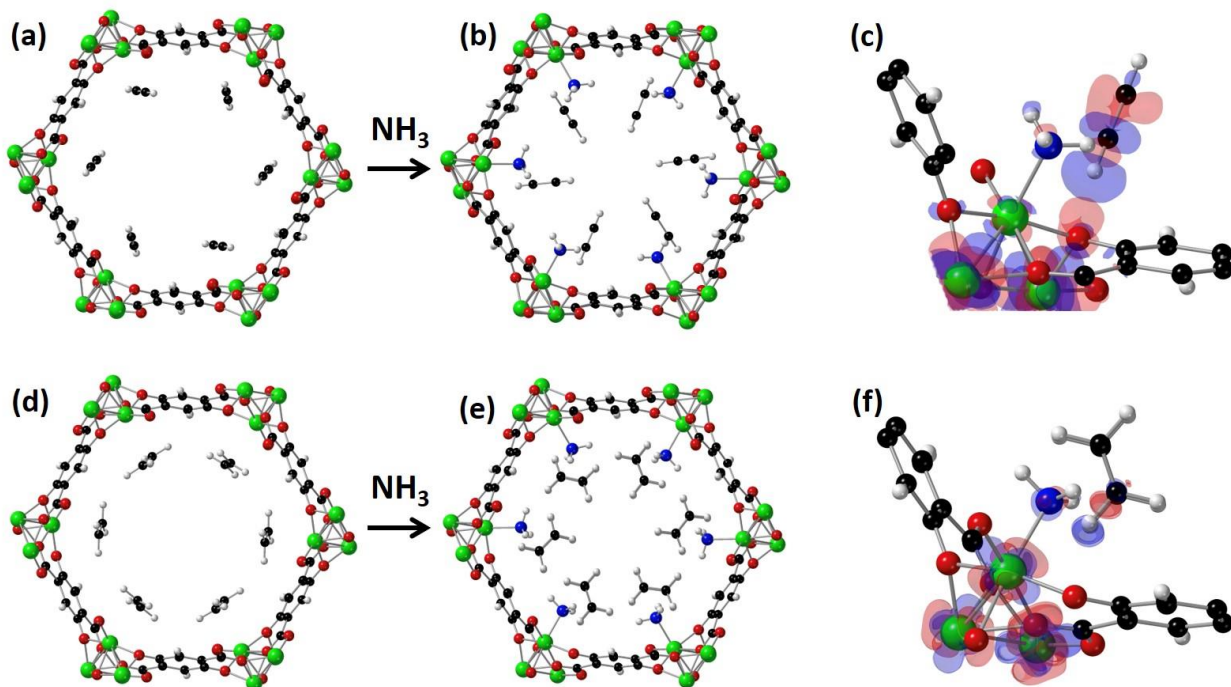


Figure 3. Configuration of C_2H_2 and C_2H_4 bound in pristine (a, d) and NH_3 loaded (b, e) Co-MOF-74. Color scheme: Green = Co, red = O, black = C, blue = N, white = H. Panel (c) and (f) show the induced charge densities of C_2H_2 and C_2H_4 co-adsorbed with the metal-bound NH_3 .

mixture and only a tiny peak of adsorbed C_2H_4 was detected in the difference spectra (less than 10% of the intensity from single-phase measurement in $NH_3@Co-MOF-74$ and less than 3% of pristine Co-MOF-74). In stark contrast, the adsorption uptake and rate of C_2H_4 in the gas-mixture is almost unaffected, as seen by the evolution of the $\delta(C_2H_2)$ band at 764 cm^{-1} in Figure 2c. The C_2H_2/C_2H_4 co-adsorption behavior in $NH_3@Co-MOF-74$ is also markedly different from pristine Co-MOF-74, which adsorbs comparable amounts of C_2H_4 and C_2H_2 due to similarity of their binding energies and diffusion barriers. To validate the role of NH_3 in the preferential adsorption of C_2H_2 over C_2H_4 , we perform experiments on Mg-MOF-74 in a like manner, which shows similar results (see Fig. S9). All the spectroscopic evidence shown in Figure S9 suggests that co-adsorbed NH_3 , instead of the metal center, plays a dominant role in controlling mixed gas C_2H_2/C_2H_4 co-adsorption in MOF-74 materials.

To gain mechanistic, molecular-level understanding of what causes this dramatic change in molecular co-adsorption behavior upon loading NH_3 , we turn to *ab initio* calculations. Our calculations show that in the pristine MOF the binding energy for C_2H_2 and C_2H_4 alone is 48.3 and 48.0 kJ/mol (see Table S2), respectively, which is in good agreement with the experimental values of ~ 50.1 and ~ 47 kJ/mol.¹⁷⁻¹⁸ The calculated binding energy of NH_3 in the pristine MOF is 73 kJ/mol and thus significantly stronger than the binding of both hydrocar-

bons, guaranteeing that NH_3 remains bound in mixtures of these gases (see Fig 2b). To further investigate these interactions, we calculate the *induced* charge density as the difference between the total and individual (pristine Co-MOF-74/ $NH_3@Co-MOF-74$ and guest molecules) charge densities, indicating the charge density rearrangement upon formation of the bond. We see that both guest molecules adsorb parallel to the channel axis and make a strong bond with the metal-center via C-Co (see Fig. 3a, 3d and S9). The very similar induced charge densities explain the very similar binding energies (see Fig. S10). We next calculate the binding energies of C_2H_2 and C_2H_4 in $NH_3@Co-MOF-74$. In both cases, the hydrocarbons now bind near to the pre-adsorbed NH_3 (see Fig. 3b and 3e), however, C_2H_2 now has a noticeable higher binding energy of 50.3 kJ/mol compared to C_2H_4 with a binding energy of only 41.7 kJ/mol (see Table S2). Clearly, the host-guest interaction is altered by the presence of NH_3 . The guest molecules C_2H_2 and C_2H_4 now make one hydrogen bond with NH_3 via their π electron clouds and another stronger one with the O via C-H (see Fig. 3c and 3f). In addition, we see a greater charge transfer in C_2H_2 compared with C_2H_4 in Figs. 3c and 3f due to its stronger acidity,⁴⁷ thus explaining the favorable binding of the former molecule over the latter one. We also see the alteration in adsorption orientation for both guest molecules affected by the presence of NH_3 . Particularly, C_2H_2 now binds perpendicular to the channel axis and occupies most of the available space,

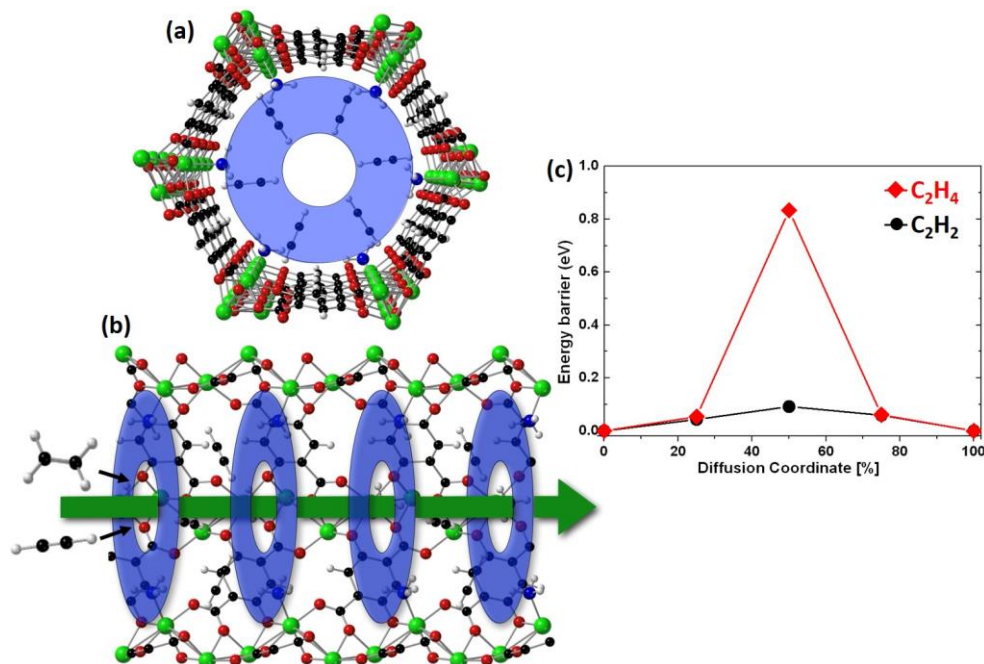


Figure 4. Energy profile for diffusion of C_2H_2 and C_2H_4 through the channel of Co-MOF-74 occupied with NH_3 and C_2H_2 . The diffusion is modeled along the channel direction through one of the apertures (inner white circle) made by the bound NH_3 and C_2H_2 molecules (outer blue circle) in panel (a) and (b). The peak positions are located at 0.09 and 0.83 eV in panel (c), corresponding to the configuration where the guest molecule is exactly inside the aperture.

forming another smaller channel and thus restricting the diffusion of the larger C_2H_4 molecule, see Fig. 4. We thus calculate the kinetics of molecular diffusion in the presence of NH_3 . Due to its smaller size and high binding energy, C_2H_2 will diffuse and occupy the outer region of MOF-74 channel prior to C_2H_4 . C_2H_2 will then take on the configuration shown in Fig. 4a in close proximity to NH_3 in such a way as to significantly reduce the channel cross section (pore opening). Using a transition-state search algorithm, we calculate the diffusion barrier of both hydrocarbons through the remaining hole in the middle of the channel (see Fig. 4c). For C_2H_2 , we find a self-diffusion barrier of 8.9 kJ/mol (~ 0.09 eV). This relatively low barrier is a result of the linear shape and corresponding small kinetic diameter of C_2H_2 (3.3 Å) and can easily be overcome at room temperature, allowing C_2H_2 to diffuse readily into the bulk of MOFs crystallites. On the other hand, for C_2H_4 we find an almost ten times larger diffusion barrier of 80.4 kJ/mol (~ 0.83 eV). This large barrier is the result of the noticeably larger kinetic diameter of C_2H_4 (3.9 Å) and is much harder to overcome at room temperature, explaining the experimentally observed dramatic drop in C_2H_4 uptake compared to C_2H_2 in the measurement of mixed gases adsorption within $NH_3@Co-MOF-74$ (see Fig. 2b and 2c).

Conclusion

In conclusion, we show a novel example of tuning the adsorption behavior of nano-porous MOF through intro-

ducing co-adsorbed species. In particular, we show that the pristine MOF-74 structure cannot discriminate between C_2H_2 and C_2H_4 molecules. However, after loading NH_3 into MOF-74, this structure shows significant C_2H_2 uptake and almost no C_2H_4 uptake in gas mixture experiment due to the modification of both their binding energy and kinetic diffusion barrier. Our finding constitutes a paradigm shift in the search for selective MOFs—rather than finding entirely new MOF structures that requires tedious synthetic attempts, we can now simply turn previously unselective MOFs into selective ones by pre-loading tightly-bound “selector” molecules (see the similar results in another well-known material HKUST-1 in Fig S.11). The advantage of our new approach is that we can choose from a vast array of already well-characterized MOFs with known routes to synthesis and physical/chemical properties such as stability, pore size/distribution, and morphology.

Supporting information:

Sample preparation and characterization; *in situ* IR spectroscopy and *ab initio* calculation methods; IR spectra of C_2H_2 , C_2H_4 adsorption into pristine and $NH_3@Co-MOF-74$ in the single and mixed gas phase. Charge density of C_2H_2 and C_2H_4 at the metal center of Co-MOF-74.

AUTHOR INFORMATION:

Kui Tan: kuitan@utdallas.edu

Timo Thonhauser: thonhauser@wfu.edu

Author Contributions:

E. C. and S. U. contributed equally to this work.

Notes:

The authors declare no competing financial interests.

Acknowledgments:

This work was supported in full by the U.S. Department of Energy, Office of Science, Office of Basic Energy Sciences under Award No. DE-SC0019902.

References:

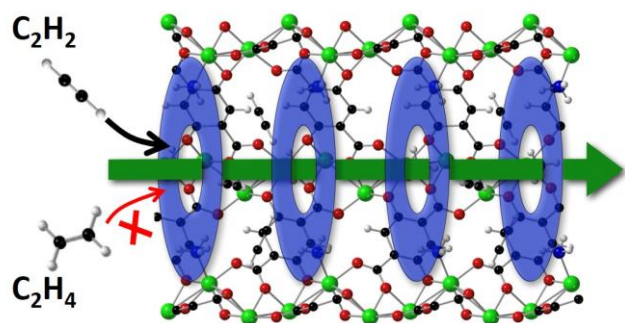
1. Broom, D. P.; Thomas, K. M., Gas Adsorption by Nanoporous Materials: Future Applications and Experimental Challenges. *MRS Bulletin* **2013**, *38* (05), 412-421.
2. Tan, K.; Zuluaga, S.; Gong, Q.; Gao, Y.; Nijem, N.; Li, J.; Thonhauser, T.; Chabal, Y. J., Competitive Coadsorption of CO₂ with H₂O, NH₃, SO₂, NO, NO₂, N₂, O₂, and CH₄ in M-MOF-74 (M = Mg, Co, Ni): The Role of Hydrogen Bonding. *Chemistry of Materials* **2015**, *27* (6), 2203-2217.
3. Sumida, K.; Rogow, D. L.; Mason, J. A.; McDonald, T. M.; Bloch, E. D.; Herm, Z. R.; Bae, T.-H.; Long, J. R., Carbon Dioxide Capture in Metal–Organic Frameworks. *Chemical Reviews* **2011**, *112* (2), 724-781.
4. Hamon, L.; Llewellyn, P. L.; Devic, T.; Ghoufi, A.; Clet, G.; Guillerm, V.; Pirngruber, G. D.; Maurin, G.; Serre, C.; Driver, G.; van Beek, W.; Jolimaître, E.; Vimont, A.; Daturi, M.; Férey, G., Co-adsorption and Separation of CO₂–CH₄ Mixtures in the Highly Flexible MIL-53(Cr) MOF. *Journal of the American Chemical Society* **2009**, *131* (47), 17490-17499.
5. Kundu, A.; Sillar, K.; Sauer, J., Predicting Adsorption Selectivities From Pure Gas Isotherms for Gas Mixtures in Metal–Organic Frameworks. *Chemical Science* **2020**, *11* (3), 643-655.
6. You, W.; Liu, Y.; Howe, J. D.; Sholl, D. S., Competitive Binding of Ethylene, Water, and Carbon Monoxide in Metal–Organic Framework Materials with Open Cu Sites. *The Journal of Physical Chemistry C* **2018**, *122* (16), 8960-8966.
7. McDonald, T. M.; Mason, J. A.; Kong, X.; Bloch, E. D.; Gygi, D.; Dani, A.; Crocellà, V.; Giordanino, F.; Odoh, S. O.; Drisdell, W. S.; Vlasisavljevich, B.; Dzubak, A. L.; Poloni, R.; Schnell, S. K.; Planas, N.; Lee, K.; Pascal, T.; Wan, L. F.; Prendergast, D.; Neaton, J. B.; Smit, B.; Kortright, J. B.; Gagliardi, L.; Bordiga, S.; Reimer, J. A.; Long, J. R., Cooperative Insertion of CO₂ in Diamine-Appended Metal–Organic Frameworks. *Nature* **2015**, *519* (7543), 303-308.
8. Burtch, N. C.; Walton, I. M.; Hungerford, J. T.; Morelock, C. R.; Jiao, Y.; Heinen, J.; Chen, Y.-S.; Yakovenko, A. A.; Xu, W.; Dubbeldam, D.; Walton, K. S., In situ Visualization of Loading-Dependent Water Effects in a Stable Metal–Organic Framework. *Nature Chemistry* **2020**, *12* (2), 186-192.
9. Rieth, A. J.; Wright, A. M.; Dincă, M., Kinetic Stability of Metal–Organic Frameworks for Corrosive and Coordinating Gas Capture. *Nature Reviews Materials* **2019**, *4* (11), 708-725.
10. Grant Glover, T.; Peterson, G. W.; Schindler, B. J.; Britt, D.; Yaghi, O., MOF-74 Building Unit Has a Direct Impact On Toxic Gas Adsorption. *Chemical Engineering Science* **2011**, *66* (2), 163-170.
11. Canivet, J.; Fateeva, A.; Guo, Y.; Coasne, B.; Farrusseng, D., Water Adsorption In MOFs: Fundamentals and Applications. *Chemical Society Reviews* **2014**, *43* (16), 5594-5617.
12. Burtch, N. C.; Jasuja, H.; Walton, K. S., Water Stability and Adsorption in Metal–Organic Frameworks. *Chemical Reviews* **2014**, *114* (20), 10575-10612.
13. Zhou, W.; Zhang, Z.; Wang, H.; Yan, Y.; Liu, X., Molecular Insights into Competitive Adsorption of CO₂/CH₄ Mixture in Shale Nanopores. *RSC Advances* **2018**, *8* (59), 33939-33946.
14. Huang, H.; Zhang, W.; Liu, D.; Zhong, C., Understanding the Effect of Trace Amount of Water on CO₂ Capture in Natural Gas Upgrading in Metal–Organic Frameworks: A Molecular Simulation Study. *Industrial & Engineering Chemistry Research* **2012**, *51* (30), 10031-10038.
15. Tan, K.; Jensen, S.; Zuluaga, S.; Chapman, E. K.; Wang, H.; Rahman, R.; Cure, J.; Kim, T.-H.; Li, J.; Thonhauser, T.; Chabal, Y. J., Role of Hydrogen Bonding on Transport of Coadsorbed Gases in Metal–Organic Frameworks Materials. *Journal of the American Chemical Society* **2018**, *140* (3), 856-859.
16. Caskey, S. R.; Wong-Foy, A. G.; Matzger, A. J., Dramatic Tuning of Carbon Dioxide Uptake via Metal Substitution in a Coordination Polymer with Cylindrical Pores. *Journal of the American Chemical Society* **2008**, *130* (33), 10870-10871.
17. Liao, Y.; Zhang, L.; Weston, M. H.; Morris, W.; Hupp, J. T.; Farha, O. K., Tuning Ethylene Gas Adsorption via Metal Node Modulation: Cu-MOF-74 for a High Ethylene Deliverable Capacity. *Chemical Communications* **2017**, *53* (67), 9376-9379.
18. Xiang, S.; Zhou, W.; Zhang, Z.; Green, M. A.; Liu, Y.; Chen, B., Open Metal Sites within Isostructural Metal–Organic Frameworks for Differential Recognition of Acetylene and Extraordinarily High Acetylene Storage Capacity at Room Temperature. *Angewandte Chemie International Edition* **2010**, *49* (27), 4615-4618.
19. Tan, K.; Zuluaga, S.; Fuentes, E.; Mattson, E. C.; Veyan, J.-F.; Wang, H.; Li, J.; Thonhauser, T.; Chabal, Y. J., Trapping Gases in Metal Organic Frameworks With a Selective Surface Molecular Barrier Layer. *Nature Communications* **2016**, *7*, 13871.
20. Tan, K.; Jensen, S.; Wang, H.; Feng, L.; Wei, K.; Zhou, H.-C.; Li, J.; Thonhauser, T., Thermally Activated Adsorption in Metal–Organic Frameworks with a Temperature-Tunable Diffusion Barrier Layer. *Angewandte Chemie International Edition* **2020**, *59* (42), 18468-18472.
21. Li, L.; Lin, R.-B.; Krishna, R.; Li, H.; Xiang, S.; Wu, H.; Li, J.; Zhou, W.; Chen, B., Ethane/Ethylene Separation In a Metal–Organic Framework With Iron-Peroxo Sites. *Science* **2018**, *362* (6413), 443.

22. Bloch, E. D.; Queen, W. L.; Krishna, R.; Zadrozny, J. M.; Brown, C. M.; Long, J. R., Hydrocarbon Separations in a Metal-Organic Framework with Open Iron(II) Coordination Sites. *Science* **2012**, *335* (6076), 1606-1610.
23. Nijem, N.; Canepa, P.; Kaipa, U.; Tan, K.; Roodenko, K.; Tekarli, S.; Halbert, J.; Oswald, I. W. H.; Arvapally, R. K.; Yang, C.; Thonhauser, T.; Omary, M. A.; Chabal, Y. J., Water Cluster Confinement and Methane Adsorption in the Hydrophobic Cavities of a Fluorinated Metal-Organic Framework. *Journal of the American Chemical Society* **2013**, *135* (34), 12615-12626.
24. Zuluaga, S.; Fuentes-Fernandez, E. M. A.; Tan, K.; Li, J.; Chabal, Y. J.; Thonhauser, T., Cluster Assisted Water Dissociation Mechanism in MOF-74 and Controlling It Using Helium. *Journal of Materials Chemistry A* **2016**, *4* (29), 11524-11530.
25. Chmelik, C.; Mundstock, A.; Dietzel, P. D. C.; Caro, J., Idiosyncrasies of CO₂(dhtp): In situ-Annealing by Methanol. *Microporous and Mesoporous Materials* **2014**, *183*, 117-123.
26. Deng, H.; Grunder, S.; Cordova, K. E.; Valente, C.; Furukawa, H.; Hmadeh, M.; Gándara, F.; Whalley, A. C.; Liu, Z.; Asahina, S.; Kazumori, H.; O’Keeffe, M.; Terasaki, O.; Stoddart, J. F.; Yaghi, O. M., Large-Pore Apertures in a Series of Metal-Organic Frameworks. *Science* **2012**, *336* (6084), 1018.
27. Dietzel, P. D. C.; Johnsen, R. E.; Fjellvag, H.; Bordiga, S.; Groppo, E.; Chavan, S.; Blom, R., Adsorption Properties and Structure of CO₂ Adsorbed on Open Coordination Sites of Metal-Organic Framework Ni₂(dhtp) from Gas Adsorption, IR Spectroscopy and X-ray Diffraction. *Chemical Communications* **2008**, (41), 5125 - 5127.
28. Britt, D.; Tranchemontagne, D.; Yaghi, O. M., Metal-Organic Frameworks With High Capacity and Selectivity For Harmful Gases. *Proceedings of the National Academy of Sciences* **2008**, *105* (33), 11623-11627.
29. Perry, J. J.; Teich-McGoldrick, S. L.; Meek, S. T.; Greathouse, J. A.; Haranczyk, M.; Allendorf, M. D., Noble Gas Adsorption in Metal-Organic Frameworks Containing Open Metal Sites. *The Journal of Physical Chemistry C* **2014**, *118* (22), 11685-11698.
30. Yazaydin, A. O. z. r.; Snurr, R. Q.; Park, T.-H.; Koh, K.; Liu, J.; LeVan, M. D.; Benin, A. I.; Jakubczak, P.; Lanuza, M.; Galloway, D. B.; Low, J. J.; Willis, R. R., Screening of Metal-Organic Frameworks for Carbon Dioxide Capture from Flue Gas Using a Combined Experimental and Modeling Approach. *Journal of the American Chemical Society* **2009**, *131* (51), 18198-18199.
31. Wu, X.; Bao, Z.; Yuan, B.; Wang, J.; Sun, Y.; Luo, H.; Deng, S., Microwave Synthesis and Characterization of MOF-74 (M=Ni, Mg) for Gas Separation. *Microporous and Mesoporous Materials* **2013**, *180*, 114-122.
32. Kresse, G.; Furthmüller, J., Efficient Iterative Schemes for ab initio Total-Energy Calculations Using a Plane-Wave Basis Set. *Physical Review B* **1996**, *54* (16), 11169-11186.
33. Kresse, G.; Joubert, D., From Ultrasoft Pseudopotentials to the Projector Augmented-wave Method. *Physical Review B* **1999**, *59* (3), 1758-1775.
34. Berland, K.; Cooper, V. R.; Lee, K.; Schröder, E.; Thonhauser, T.; Hyldgaard, P.; Lundqvist, B. I., Van Der Waals Forces in Density Functional Theory: a Review of the vdW-DF Method. *Reports on Progress in Physics* **2015**, *78* (6), 066501.
35. Langreth, D. C.; Lundqvist, B. I.; Chakarova-Kack, S. D.; Cooper, V. R.; Dion, M.; Hyldgaard, P.; Kelkkanen, A.; Kleis, J.; Kong, L.; Li, S.; Moses, P. G.; Murray, E.; Puzder, A.; Rydberg, H.; Schroder, E.; Thonhauser, T., A Density Functional For Sparse Matter. *Journal of Physics: Condensed Matter* **2009**, *21*, 084203.
36. Thonhauser, T.; Cooper, V. R.; Li, S.; Puzder, A.; Hyldgaard, P.; Langreth, D. C., Van Der Waals Density Functional: Self-Consistent Potential and the Nature of the Van Der Waals Bond. *Physical Review B* **2007**, *76* (12), 125112.
37. Thonhauser, T.; Zuluaga, S.; Arter, C. A.; Berland, K.; Schröder, E.; Hyldgaard, P., Spin Signature of Nonlocal Correlation Binding in Metal-Organic Frameworks. *Physical Review Letters* **2015**, *115* (13), 136402.
38. Canepa, P.; Nijem, N.; Chabal, Y. J.; Thonhauser, T., Diffusion of Small Molecules in Metal Organic Framework Materials. *Physical Review Letters* **2013**, *110* (2), 026102.
39. Henkelman, G.; Uberuaga, B. P.; Jónsson, H., A Climbing Image Nudged Elastic Band Method for Finding Saddle Points and Minimum Energy Paths. *The Journal of Chemical Physics* **2000**, *113* (22), 9901-9904.
40. Henkelman, G.; Jónsson, H., Improved Tangent Estimate in the Nudged Elastic Band Method for Finding Minimum Energy Paths and Saddle Points. *The Journal of Chemical Physics* **2000**, *113* (22), 9978-9985.
41. Iwashita, Y.; Tamura, F.; Nakamura, A., Spectroscopic Studies on Coordinated Acetylene. *Inorganic Chemistry* **1969**, *8* (5), 1179-1183.
42. Bonino, F.; Chavan, S.; Vitillo, J. G.; Groppo, E.; Agostini, G.; Lamberti, C.; Dietzel, P. D. C.; Prestipino, C.; Bordiga, S., Local Structure of CPO-27-Ni Metallorganic Framework upon Dehydration and Coordination of NO. *Chemistry of Materials* **2008**, *20* (15), 4957-4968.
43. Nijem, N.; Canepa, P.; Kong, L. Z.; Wu, H. H.; Li, J.; Thonhauser, T.; Chabal, Y. J., Spectroscopic Characterization of Van Der Waals Interactions in a Metal Organic Framework with Unsaturated Metal Centers: MOF-74-Mg. *Journal of Physics-Condensed Matter* **2012**, *24* (42), 424203.
44. Lamberti, C.; Zecchina, A.; Groppo, E.; Bordiga, S., Probing the Surfaces of Heterogeneous Catalysts by in situ IR Spectroscopy. *Chemical Society Reviews* **2010**, *39* (12), 4951-5001.
45. Gussoni, M.; castiglioni, C.; Ramos, M. N.; Rui, M.; Zerbi, G. Z., Infrared Intensity: from Intensity Parameters to an Overall Understanding of the Spectrum. *Journal of Molecular Spectroscopy* **1990**, *224*, 445-470.

46. Nakamoto, K., *Infrared and Raman Spectra of Inorganic and Coordination Compounds*, 6th ed. **2009**, Wiley & Sons, Inc. Hoboken, New Jersey, United States.

47. Nijem, N.; Wu, H. H.; Canepa, P.; Marti, A.; Balkus, K. J.; Thonhauser, T.; Li, J.; Chabal, Y. J., Tuning the Gate Opening Pressure of Metal-Organic Frameworks (MOFs) for the Selective Separation of Hydrocarbons. *Journal of the American Chemical Society* **2012**, 134 (37), 15201-15204.

TOC



— Supporting Information —

Tuning the Adsorption Properties of Metal-Organic Frameworks through Co-adsorbed Ammonia

Eric Chapman,^{1†} Saif Ullah,^{1†} Hao Wang,² Liang Feng,³ Kunyu Wang,³ Hong-Cai Zhou,³ Jing Li,² Timo Thonhauser,^{1*} and Kui Tan^{4*}

¹Department of Physics and Center for Functional Materials, Wake Forest University, Winston-Salem, NC 27109

²Department of Chemistry and Chemical Biology, Rutgers University, Piscataway, NJ 08854

³Department of Chemistry, Texas A&M University, College Station, TX 77843

⁴Department of Materials Science & Engineering, University of Texas at Dallas, Richardson, TX 75080

*Kui Tan: kuitan@utdallas.edu

*Timo Thonhauser: thonhauser@wfu.edu

Table of Contents

1. Physical characterization of MOFs samples.....	3
2. IR spectra of adsorbed NH ₃ , C ₂ H ₂ and C ₂ H ₄ in Co-MOF-74	4
3. IR spectra of adsorbed C ₂ H ₂ and C ₂ H ₄ in NH ₃ @Co, Mg-MOF-74.....	7
4. Configuration of adsorbed C ₂ H ₂ and C ₂ H ₄ in pristine Co-MOF-74	9
5. Assignment of infrared bands.....	10
6. Calculated binding energy	10
7. C ₂ H ₂ and C ₂ H ₄ adsorption in pristine and NH ₃ @HKUST-1	11

1. Physical characterization of MOFs samples

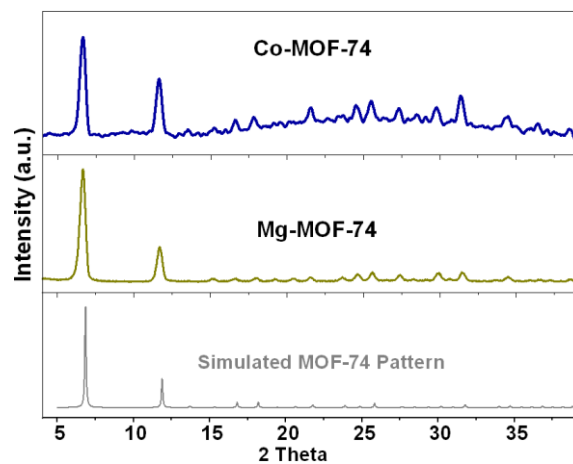


Figure S1. Powder X-ray diffraction pattern of Mg-MOF-74 and Co-MOF-74 sample (after solvent exchange) with the simulated pattern from single crystal data of Ni-MOF-74 (*Chemical Communications* 2008, 41, 5125 - 5127).

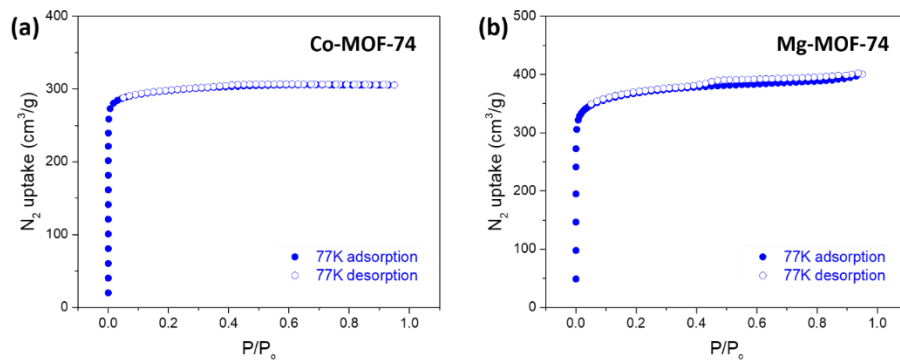


Figure S2. N₂ adsorption isotherm in Co-MOF-74 (a) and Mg-MOF-74 (b) at 77 K.

2. IR spectra of adsorbed NH₃, C₂H₂ and C₂H₄ in Co-MOF-74

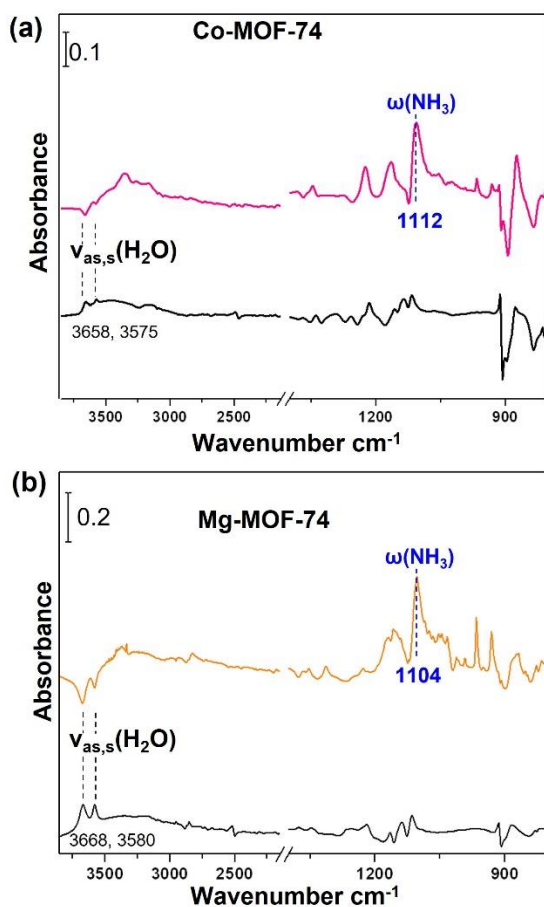


Figure S3. IR spectra of loading NH₃ into slightly hydrated (a) Co- and (b) Mg-MOF-74 samples that were pre-loaded with H₂O at ~500 mTorr, in comparison with the spectrum prior to NH₃ adsorption. Once NH₃ (~50 Torr) was introduced, a quick loss of water bands including v_{as,s}(H₂O) was observed, indicating pre-adsorbed H₂O at the metal sites can be readily displaced by post-loaded NH₃, characterized by growth of its wagging band around 1100 cm⁻¹.

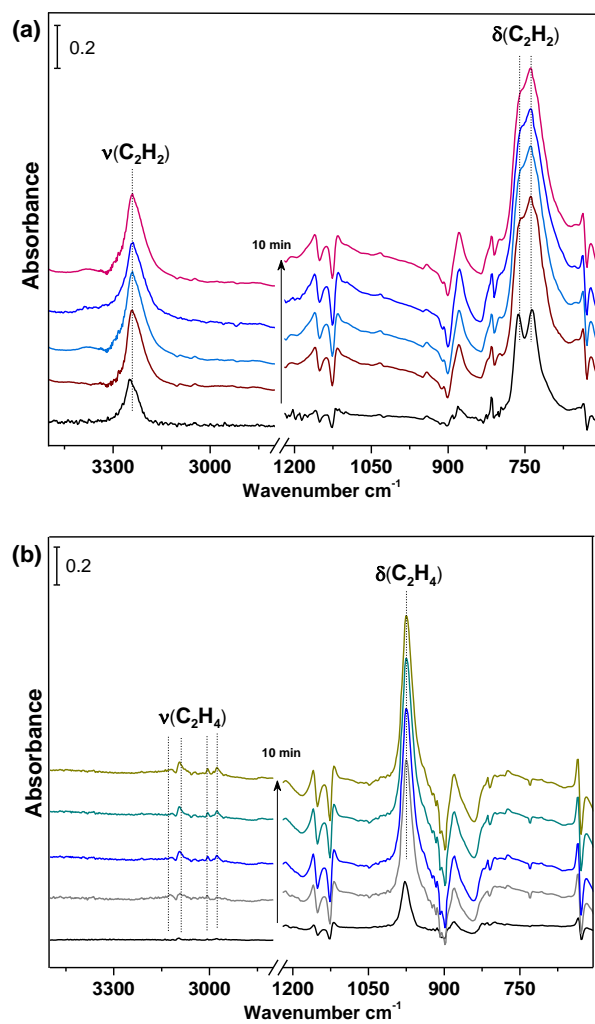


Figure S4. IR spectra of C_2H_2 (a) and C_2H_4 (b) adsorption into pristine Co-MOF-74 upon loading their single components of gas phase at ~ 200 Torr as a function of time.

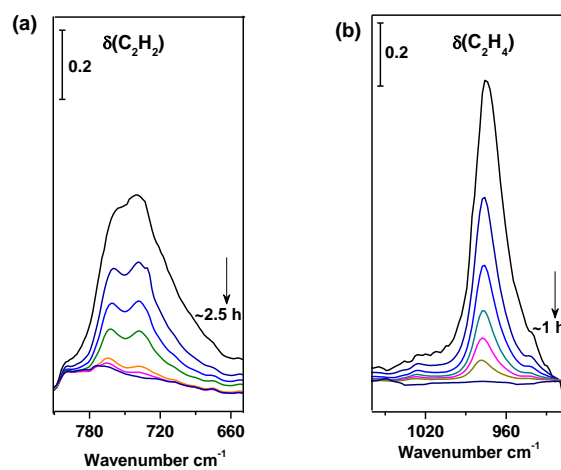


Figure S5. IR spectra of C_2H_2 (a) and C_2H_4 (b) desorption from pristine Co-MOF-74 as a function of time.

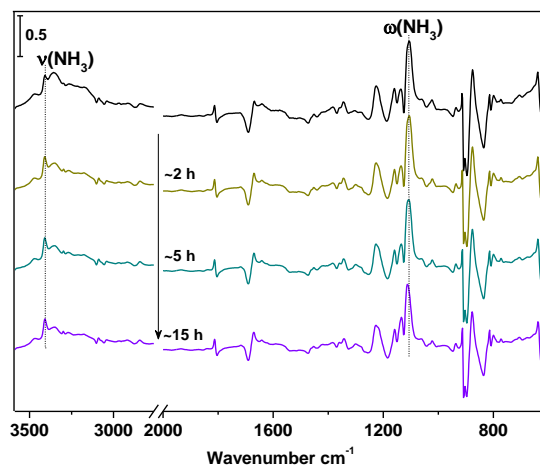


Figure S6. IR spectra of adsorbed NH_3 (loaded at ~ 50 Torr) in Co-MOF-74 upon evacuation process under vacuum.

3. IR spectra of adsorbed C₂H₂ and C₂H₄ in NH₃@Co, Mg-MOF-74

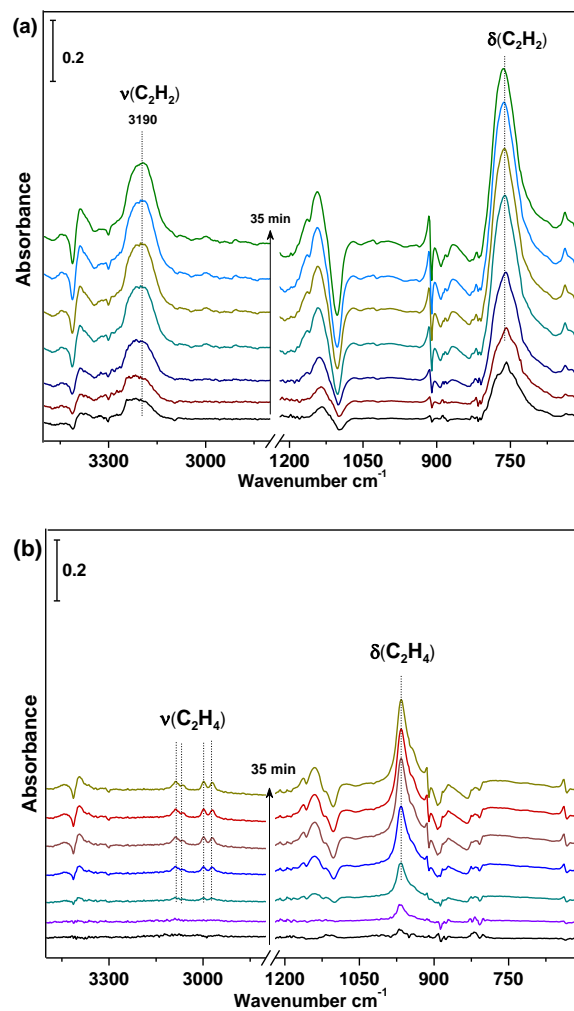


Figure S7. IR spectra of C₂H₂ (a) and C₂H₄ (b) adsorption into NH₃@Co-MOF-74 upon loading their single components of gas phase at ~200 Torr as a function of time.

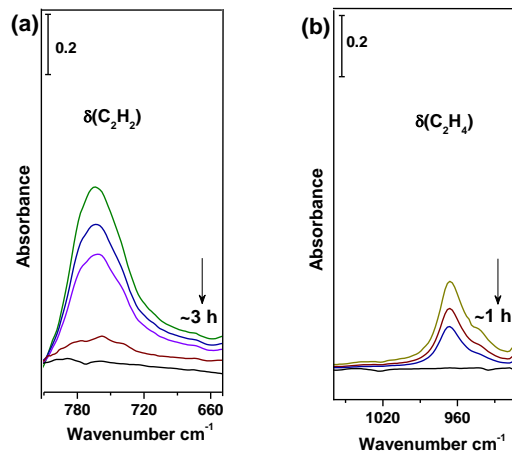


Figure S8. IR spectra of C_2H_2 (a) and C_2H_4 (b) desorption from $NH_3@Co-MOF-74$ as a function of time.

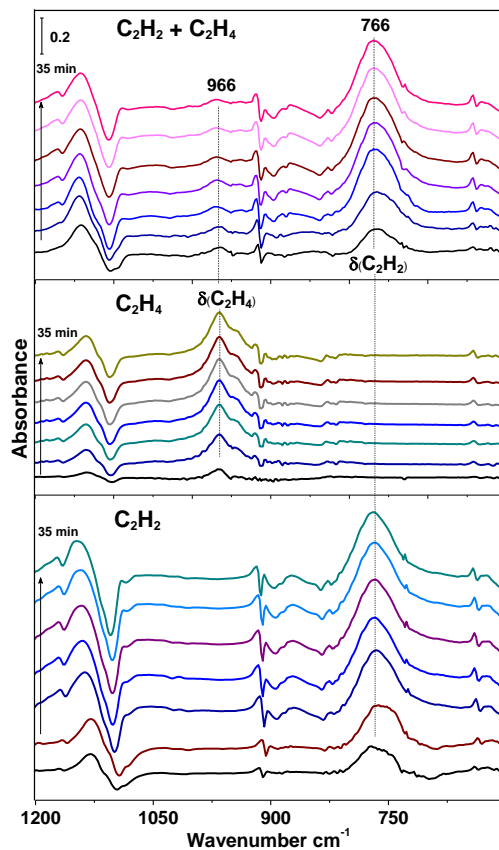


Figure S9. Spectral evolution of the deformation band δ of adsorbed C_2H_2 and C_2H_4 molecules in NH_3 -loaded $Mg-MOF-74$ upon exposure to single C_2H_2 (bottom) and C_2H_4 (middle) at 200 Torr, and mixed C_2H_2/C_2H_4 at 200 Torr/200 Torr (top).

4. Configuration of adsorbed C₂H₂ and C₂H₄ in pristine Co-MOF-74

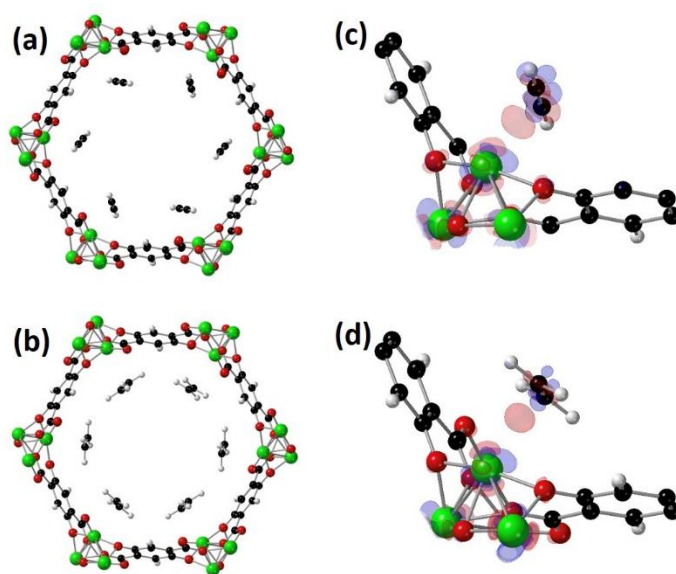


Figure S10. Induced charge density isosurface with isovalue of $0.003 \text{ e}/\text{\AA}^3$ for C₂H₂ (a, c) and C₂H₄ (b, d) at the metal center of Co-MOF-74. Color scheme: Green = Co, red = O, black = C, blue = N, white = H.

5. Assignment of infrared bands

Table S1. Assignment of infrared bands of pristine Co-MOF-74 observed in Figure 2d.

IR bands	Position
$\nu(\text{C-O})$ of phenolate	1198
$\delta(\text{CH})_{\text{ip}}$	1154
	1123
$\gamma(\text{CH})_{\text{oop}}$	889
$\beta(\text{COO})_{\text{as}}$	825

Notation and acronyms: ν , stretching; β , scissoring; δ and γ , deformation; ip, in plane; oop, out of plane.

6. Calculated binding energy

Table S2. Calculated binding energy (kJ/mol) of C_2H_2 and C_2H_4 in pristine and $\text{NH}_3@$ Co-MOF-74.

	C_2H_2	C_2H_4
Co-MOF-74	48.3	48.0
$\text{NH}_3@$ Co-MOF-74	50.3	41.7

7. C₂H₂ and C₂H₄ adsorption in pristine and NH₃@HKUST-1

We have explored the binding of C₂H₂/C₂H₄ in another well-known MOF material, i.e. HKUST-1 (*Science*, 1999, 283, 1148-1150), before and after binding NH₃ (see Figure S11). Without the presence of NH₃ as selector molecule, C₂H₂/C₂H₄ occupy the same open metal sites (Cu²⁺) and bind along the chamber (parallel to the pore axis), in the same way as we observe in MOF-74. However, when NH₃ is introduced as selector, all the metal sites are occupied by NH₃, and the C₂H₂/C₂H₄ guest molecules follow an adsorption pattern quite similar to that of MOF-74. Due to the absence of any open metal sites, guest molecules now bind perpendicular to the pore axis and near the vicinity of the selector. In this case, the binding energies of C₂H₂ and C₂H₄ become 29 and 27 kJ/mol, respectively, showing that C₂H₂ will bind more favorably than C₂H₄. Consequently, the adsorbed C₂H₂ molecules form an additional diffusion barrier by occupying a significant amount of the pore. In striking similarity with MOF-74, C₂H₄ is excluded due to its larger size (kinetic effect), and the MOF will only uptake C₂H₂ as observed by mimicking the energy barrier calculations. This suggests that our observation may be applicable more generally to MOFs with comparable pore diameter and open metal sites.

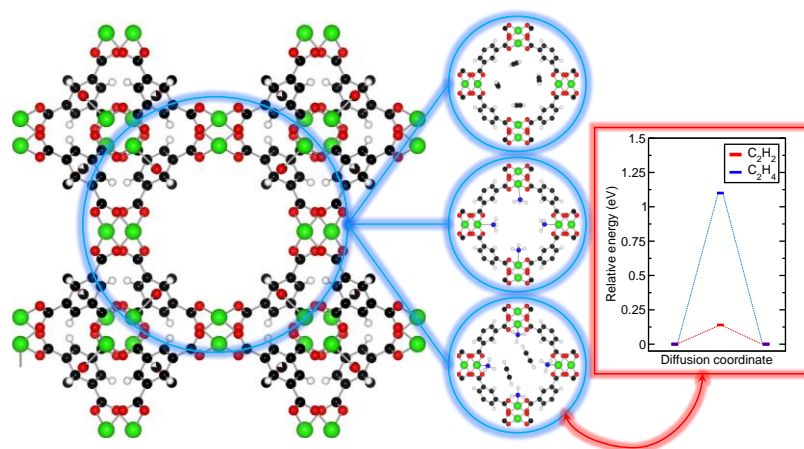


Figure S11. Geometric structure of empty HKUST-1. C₂H₂ adsorption pattern in HKUST-1 occupying the open metal sites (top inset). NH₃ binding at the open metal sites (middle inset) and C₂H₂ adsorption pattern in the presence of the NH₃ selector (bottom inset). In the latter conformation, C₂H₂ adopts a distinct binding pattern, narrowing the pore size and excluding bigger molecules such as C₂H₄ from entering the pore as shown by the energy barrier calculations. For C₂H₂, a barrier of 0.14 eV is calculated, which can easily be overcome at room temperature. However, a huge diffusion barrier of 1.1 eV prevents C₂H₄ uptake by molecular sieving.